POST-PROJECTION REMOVAL OF ROW- AND COLUMN-CORRELATED NOISE IN LINE-SCANNING DATA: APPLICATION TO THEMIS INFRARED DATA

K. J. Nowicki[1], C. S. Edwards[2], P. R. Christensen[3]

[1]Southwest Research Institute, Boulder, CO (keith.nowicki@swri.org); [2]California Institute of Technology, Pasadena, CA; [3]Arizona State University, Tempe, AZ.

ABSTRACT

Post-calibration row- and column-correlated noise resulting from voltage instability in the electronics of the Thermal Emission Imaging System (THEMIS), on-board the 2001 Mars Odyssey spacecraft is mapped with the data during map projection, making reliable spectral analysis of small areas (< 4km^2) problematic. The majority of detector-row and column correlated noise is removed during calibration using a windowed algorithm and utilizing information in the Instrument Response Function (IRF), but residual noise dubbed "plaid" and processing artifacts remain after the calibrated data has been projected. These artifacts can be readily viewed using decorrelation stretches or by numerically comparing radiance or emissivity differences in small regions. We present an algorithm to remove the residual row- and column-correlated noise from THEMIS data, leveraging post-projection information to improve the accuracy in radiance and emissivity analyses of small areas. The removal of the "plaid" is essential for the detection of spectrally significant surface materials.

Index Terms: Remote Sensing, THEMIS, Row- and Column Correlated Noise Removal

1. INTRODUCTION

Multispectral push-broom scanners are commonly used for orbital and airborne remote sensing applications. A common and significant problem with push-broom scanning systems is that they are susceptible to noise along scan-lines and detector-columns [e.g. 1, 2-4]. Minor voltage and temperature instability in the electronics of multispectral imagers produces correlated noise in the resulting imagery that makes reliable analysis of small areas (~10x10 pixels) problematic. The removal of this noise in early calibration steps is difficult or impossible due to the absence of a metric for differentiating signal from noise. Presented here is the algorithm developed for THEMIS [5] (Figure 1a-c) which has also been applied to MODIS/ASTER Simulator and (MASTER, [6], Figure 1d-f) Advanced Spaceborne Thermal Emission and Reflection Radiometer (ASTER, [7]) data. This algorithm utilizes inter-band correlations to separate row and column correlated noise from target signal with a high degree of confidence.

The initial data product created from data down-linked from the spacecraft, the Experiment Data Record (EDR), contains both vertical and horizontal stripes that are a single pixel wide. The vertical stripes, corresponding to the columns of the detector, consist of constant offsets down the EDR image with an amplitude of up to +/- 1 DN. Adjacent columns may have similar offset values, creating aggregate stripes multiple pixels in width. This column noise originates from physical differences in the construction of each detector column (e.g. marginal differences in resistances, non-homogeneity of doping, etc.) and is recorded in the IRF as part of the instrument development and calibration effort. For calibration of flight data, the detector-column noise is assumed to effectively be a constant throughout the data record. The removal of this

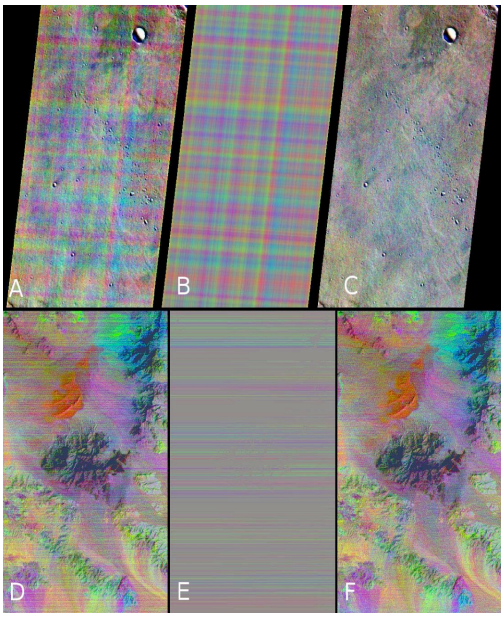

Figure 1. A) A segment of THEMIS image ID I01002002. **B)** The removed plaid retains no surface features. **C)** The deplaided data provides a better representation of the surface composition at small spatial scales. **D)** ASTER data contains the horizontal component of plaid which is similar is statistical behavior to THEMIS data. **E)** The removed plaid from ASTER data contains some surface features because the 8-bit data is saturated in either light or dark pixels. Increasing the number of bits of precision eliminates this artifact. **F)** Using the default thresholds for THEMIS results in a very good removal of plaid from MASTER data.

noise is handled through the use of the appropriate temperature index of the IRF. Residual column noise results from minor differences in detector response from the pre-launch response function [8]. The horizontal stripes are stochastic, aperiodic line-to-line noise. To first order, the origin of the noise along scan-lines is primarily due to electrical contamination of pixel row information after signal acquisition in the detector readout bias voltage during the transfer to the memory buffer. During the calibration process prior to map projection striping in the horizontal direction is removed using a windowed filtering algorithm and in the vertical direction by subtracting a scaled instrument response function.

Projected, calibrated THEMIS data contain residual detector line- and row- correlated noise that was either not removed or was introduced as an artifact of the de-striping process during calibration. Projection is an irreversible, one-to-many and many-to-one mapping process and has several effects on the data: 1) The width of the data array is no longer a constant down the image and is dependent on projection type, target distance, etc., 2) a row of pixels on the detector are mapped at some angle to the cardinal directions of the planet and consequently to the x-y coordinates of the data array because THEMIS is in a near-polar orbit and the planet is turning below it, and 3) the down-track resolution of each pixel varies because the orbiter is nutating slightly. As a result, noise that was contained to a single row or column of the data array may vary in width in the projected data. This residual noise manifests itself as bands of increased or decreased signal strength of variable width and frequency in both the vertical and horizontal directions (Fig 1A). A decorrelation stretch (DCS) is commonly used to enhance spectral variability within a scene [9]. In THEMIS DCS data, a distinct pattern of aperiodic multi-colored plaid, first characterized by [8] overlays the surface image, obscuring the color representation of the target material and making the differentiation of distinct spectral units difficult (Fig 1B).

2. METHOD

2.1 Removal of Row and Column Correlated Noise

Various techniques have been developed to remove line-to-line noises for a number of push-broom scanning instruments and to a varying degree of success and confidence, including techniques based in Fourier Analysis [e.g. 2, 4], wavelet techniques, and windowed filtering algorithms [e.g. 1]. Fourier Analysis is the predominant tool for removing well-behaved periodic signals; however, neither the row, nor the column noise in multispectral imagers like THEMIS is sufficiently periodic. Windowed filtering algorithms used without the aid of additional criteria for the accurate separation of signals are highly prone to introducing artifacts and are used only for cosmetic improvement [1, 10].

The algorithm (referred to herein as 'deplaid') was developed to remove the line- and row-correlated noise in THEMIS infrared data and uses a discriminative windowed filtering approach. Directional averages of geometrically projected data corresponding to the orientation of detector rows and columns are calculated and operated upon to extract correlated noise. The presented algorithm overcomes the intransigent shortcomings of simplistic filtering techniques by utilizing inter-band correlations and leveraging known compositional and temperature trends of the planetary surfaces.

2.2 Steps of the Deplaid Algorithm

The sequence of steps for the algorithm are as follows: 1) The data are integer pixel shifted to return to “camera coordinates” orienting the data approximately as detector rows and columns. 2) Pixels whose values deviate from the local mean by 15% are excluded to prevent the skewing of data and introduction of artifacts in filtering operations. 3) The image is divided into 500 line-segments and row and column averages are calculated. 4) The row and column averages are convolved with a high-pass sawtooth filter 150 pixels wide (3 times the maximum plaid size), as this kernel size is just sufficient to remove most plaid events. 5) The plaid radiance flux fraction is subtracted from the high-pass filtered row and column arrays to arrive at the separated plaid signal for each segment. 6) The values of column-correlated, vertical plaid are interpolated in overlapping segments to produce an evolving plaid contribution down the image. 7) The horizontal and vertical plaid are then independently subtracted from the original array to obtain noise-free radiance. 8) Finally, to remove possible residual plaid, the cleaned radiance is separated from the atmospheric radiance contribution, is converted into emissivity and each band is individually deplaided in emissivity space before being converted back into radiance.

2.3 Conservation of Radiance Flux

It is useful to construct the concept of conservation of radiance flux at the detector, or the sum of the radiance in all bands in each pixel. Conserving radiance flux during the deplaid operation requires that the sum of the plaid signal across all bands equal zero in any given pixel. This requirement implies that the distribution of plaid events follows the weak law of large numbers and converges on the mean of the distribution as the number of events goes to infinity [11]. After calculating the value of plaid in each band, the sum of the plaid radiance flux is computed and a fraction equal to the inverse of the number of bands is removed from each band. The plaid radiance flux fraction is divided evenly across bands to retain inter-band signal ratios and thereby color hue in DCS images. The plaid is thus treated as an additive noise that is irrespective of the temperature of the planetary surface. The primary strength of conserving radiance flux is that it will differentiate between a true plaid event and a feature in a THEMIS image with radiance values that are either lower or higher in all bands and whose physical extent is suggestive of a plaid

event in any single band. The requirement of conservation of radiance flux has an obvious weakness as it does nothing to correct the aggregate error introduced by plaid into sum of the radiance in all bands.

3. RESULTS

3.1 Algorithm Testing

An example of row averages of radiance data before and after the deplaid algorithm, as well as the removed plaid signal are shown in Figure 2A. High frequency information is retained during the deplaid process and sometimes is even enhanced, as shown in the shaded box. Horizontal and vertical plaid events were characterized for distribution of width and average amplitude. A plaid event was defined as a segment of the one-dimensional array (for each spectral band) of vertical or horizontal plaid contribution that are contiguous and similarly signed. Widths were measured as the distance between points where the noise function intersects zero. Statistical samplings were gathered from a collection of forty daytime THEMIS IR images selected randomly throughout the mission. The characterization of plaid was found to be independent of average image temperature, season, time of day and targeted terrain. The number of occurrences of plaid event widths declines logarithmically as width increases (Figure 2B), with a standard deviation of 11 pixels. Only 2% of all plaid events have a width of greater than 40 pixels. Amplitudes were calculated as the average spectral radiance value of all pixels within a single event. Amplitudes, in units of $W \cdot cm^{-2} \cdot \mu m^{-1} \cdot sr^{-1}$, follow a normal distribution centered on zero with standard deviation of $6e^{-7}$ and greater than 99% containment below an absolute value of $2e^{-6}$ (Figure 2C). With typical surface signals of $5e^{-5}$ to $4e^{-4}$ $W \cdot cm^{-2} \cdot \mu m^{-1} \cdot sr^{-1}$, the plaid contributes on a range of 0.15% to 4.0% of the total signal in daytime radiance data. Due to low temperatures, nighttime radiance values are often equal to the contribution of the plaid signal.

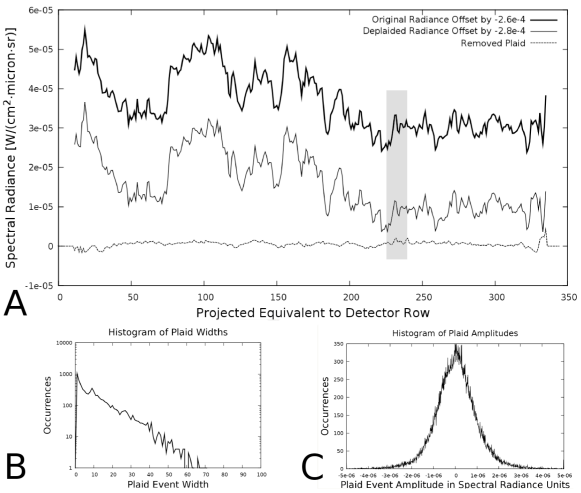

A) Row averages of radiance data before and after the deplaid algorithm, as well as the removed plaid demonstrate that unlike in a low-pass filtering scheme, high frequency information is retained during the deplaid process, as shown in the shaded boxes. **B)** A histogram of plaid widths shows a logarithmic decay with increasing width. **C)** The histogram of plaid amplitudes shows a normal distribution centered on zero.

In our test study, images were chosen from Arabia Terra and the Tharsis region because they contain large, spectrally uniform regions with little thermal variation due to shadows or thermophysical variations, and are relatively constant in elevation. Target sites with 256 pixels on a side were subdivided into sub-regions with 128, 64, 32, 16, 8 and 4 pixels on a side for which averages of emissivity were calculated. By using this method, it is possible to determine if the emissivity calculated from the average of small boxes in deplaided data better matched that of the entire region than the same boxes extracted from the original data. These improvements between the deplaided data and the original data were quantified as a difference in percentage emissivity ($\Delta\%\epsilon$) utilizing the unreduced equation:

$$\Delta\%\varepsilon = 100 \cdot \frac{\left(\left(\varepsilon_{region} - \varepsilon_{original}\right) - \left(\varepsilon_{region} - \varepsilon_{deplaided}\right)\right)}{\varepsilon_{region}}.$$

The average of each sub-region from both the original and deplaided data were subtracted from the average of the entire region. For normalization purposes, the absolute values of these quantities were converted to a percentage of the regional average. Finally, the percentage emissivity difference of the deplaided data was subtracted from that of the original data to obtain the percentage emissivity improvement in accuracy of deplaided boxes over boxes in unaltered data. Figure 3 illustrates averages and standard deviations of percentage emissivity differences between original and deplaided data for a selection of multiple sub-region sizes in a single target site. Because the scene was chosen to have uniform spectral properties and differences between boxes are due solely to plaid, positive values indicate that there was an improvement in accuracy using deplaided data. Average improvement in emissivity is on the order of 0.25% for bands 4-9 and 0.75% for bands 1 and 2. The improvement of agreement with the average of the entire region of deplaided boxes over unaltered data generally increases as sub-region size decreases. This is due to the fact that plaid events, the majority being on the order of 10 lines in width, have an increasing influence on average emissivity as sub-region size decreases. For THEMIS, this trend begins to reverse for sub-regions 4 pixels on a side. At this scale, even though plaid in the original data is still a significant contributor to error, the summation of pixel-to-pixel white noise and localized variations represent a real difference from the average of the entire target site.

4. DISCUSSION AND ERROR ANALYSIS

The deplaid algorithm achieves a high level of success for most regions of Mars but notable errors occur when surface features share defining characteristics of plaid. In particular,

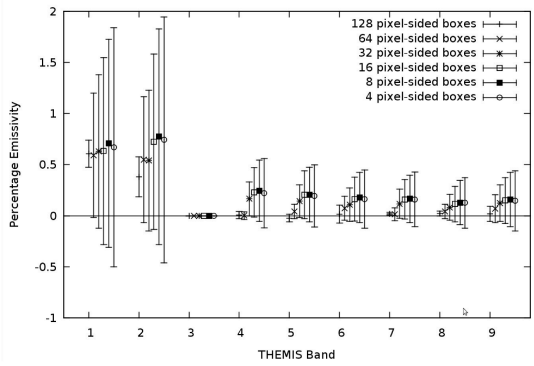

Figure 3. The difference in percentage emissivity was calculated between deplaided and original data. Positive values indicate deplaided data more accurately matched the regional average. Error bars indicate the standard deviation of all boxes of similar size. Deplaided data gains accuracy over unaltered data as box size decreases, up until a box of 4 pixels to a side.

if there exist geologic units on the surface distinct from their surroundings and they extend the width of the image or are close to 50 km long vertically and have boundaries that tend to correspond to detector rows or columns, the deplaid algorithm may be unable to differentiate between real geologic variation and plaid. In a sampling of twelve THEMIS images containing errors, the per-pixel induced errors range up to 1.2 e^{-6} $W \cdot cm^{-2} \cdot \mu m^{-1} \cdot sr^{-1}$ corresponding to an emissivity error of up to 0.4%. However, visual inspection of the image quickly reveals that this is an artifact so that algorithm errors are highly unlikely to be misinterpreted as real geologic features.

The error resulting from a similarity of surface features to plaid events is sometimes compounded by a related failure of appropriate pixel selection through insufficiently restrictive data exclusion masks. Unfortunately, surface units need not demonstrate particularly elevated or depressed total radiance flux in cases where a single band has absorption features. This makes the data exclusion mask technique ill-suited to adequately differentiate these features in THEMIS data and a more robust approach must be conceived to deal with these circumstances.

In a study of 60 daytime infrared images chosen randomly from the entire set of THEMIS images publicly available that was independent from the analyses described above, the deplaid algorithm successfully removed plaid without introducing significant errors in 58. Introduced artifacts were easily identified visually and in both cases were attributable to the failures described above. The amplitude of the errors in spectral radiance units never exceeded two standard deviations of the plaid amplitude distribution and eighty percent of the pixels inside the error event remained within one standard deviation. Furthermore, a qualitative visual inspection of three hundred DCS THEMIS false color images yielded 287 images where no error was detectable in the entire image, suggesting a success rate of greater than 95%. In the cases where errors were introduced, they occurred in small sections and were always located adjacent to surface features making them easily identifiable.

5. CONCLUSIONS

The deplaid algorithm is a robust technique to remove line- and row- correlated noise from multispectral data sets. In the case of THEMIS, it has been shown to reduce detector-derived noise error and improve the accuracy of compositional analysis of small areas with a very low rate of introducing artifacts. It also provides substantial visual improvement of false color images, facilitating spectral image interpretation. It can be applied to most multispectral images and has been shown to be effective on Earth based remote sensing data as well.

6. REFERENCES

[1] R. Crippen, "A simple spatial filtering routine for the cosmetic removal of scan-line noise from Landsat TM P-tape imagery," *Photogrammetric Engineering and Remote Sensing,* vol. 55, 327-331, 1989.

[2] C. C. Borel *et al.*, "Partial removal of correlated noise in thermal imagery," *SPIE*, 131-138, 1996.

[3] G. C. Holst, *Electro-optical imaging system performance*, 5th ed., JCD Publishing, Florida and SPIE, Washington, ch. 2, 4 and 9, 2008.

[4] T. M. Lillesand *et al.*, *Remote Sensing and Image Interpretation*, 6th ed., Wiley, New Jersey, ch. 5 and 7, 2008.

[5] P. R. Christensen *et al.*, "The Thermal Emission Imaging System (THEMIS) for the Mars 2001 Odyssey Mission," *Space Science Reviews,* vol. 110, no. 1, 85-130, 2004.

[6] S. J. Hook *et al.*, "The MODIS/ASTER airborne simulator (MASTER)-A new instrument for earth science studies," *Remote Sensing of Environment,* vol. 76, no. 1, 93-102, 2001.

[7] Y. Yamaguchi *et al.*, "Overview of Advanced Spaceborne Thermal Emission and Reflection Radiometer (ASTER)," *IEEE Transactions on Geoscience and Remote Sensing,* vol. 36, no. 4, 1062-1071, 1998.

[8] J. L. Bandfield *et al.*, "Atmospheric correction and surface spectral unit mapping using Thermal Emission Imaging System data," *J. Geophys. Res.,* vol. 109, E10008, 2004.

[9] A. R. Gillespie *et al.*, "Color enhancement of highly correlated images. I. Decorrelation and HSI contrast stretches," *Remote Sensing Environ.,* vol. 20, 209-235, 1986.

[10] J. S. Lim, *Two Dimensional Signal and Image Processing*, Prentice Hall, New Jersey, ch. 8 and 9, 1990.

[11] W. Feller, *An introduction to probability theory and its applications*, 3rd ed., Wiley, New York, ch. 10, 1968.